



# Single-step flame-made Pt/MgAl<sub>2</sub>O<sub>4</sub> – A NO<sub>x</sub> storage-reduction catalyst with unprecedented dynamic behavior and high thermal stability

Sounak Roy, Niels van Vegten, Alfons Baiker\*

Institute for Chemical and Bioengineering, Department of Chemistry and Applied Bioscience, ETH, Zurich, Hönggerberg, HCI, CH-8093 Zurich, Switzerland

## ARTICLE INFO

### Article history:

Received 31 December 2009  
Revised 8 February 2010  
Accepted 10 February 2010  
Available online 15 March 2010

### Keywords:

NO<sub>x</sub> storage and reduction  
Platinum  
Spinel  
Dynamic cycling behavior  
Time-resolved spectroscopy  
Thermal stability  
Sulfur tolerance

## ABSTRACT

One weight percentage of Pt/MgAl<sub>2</sub>O<sub>4</sub>, without any additional classical storage component (Ba or K), was synthesized by single-step flame spray pyrolysis. The catalyst consisting of nano-sized Pt dispersed on MgAl<sub>2</sub>O<sub>4</sub> spinel showed superior dynamic performance in NO<sub>x</sub> storage-reduction at short regeneration times (<30 s) compared to a standard 1%Pt–20%Ba/Al<sub>2</sub>O<sub>3</sub> reference catalyst. The better NSR performance at short regeneration times of Pt/MgAl<sub>2</sub>O<sub>4</sub> is limited to the use of hydrogen and H<sub>2</sub>–CO mixtures as reductants, whereas with other reductants, CO or C<sub>3</sub>H<sub>6</sub>, the NSR performance was similar for both catalysts. The efficiency of the reduction agents decreased in the order H<sub>2</sub> > H<sub>2</sub> + CO > CO > C<sub>3</sub>H<sub>6</sub>. XRD and time-resolved *in-situ* DRIFT investigations indicate that bulk nitrate species are formed on Pt–Ba/Al<sub>2</sub>O<sub>3</sub>, whereas on the spinel-based Pt/MgAl<sub>2</sub>O<sub>4</sub> catalyst predominantly surface species were formed. The superior dynamic performance of the spinel-based Pt/MgAl<sub>2</sub>O<sub>4</sub> is attributed to the different adsorbed NO<sub>x</sub> species and their different stability under regeneration conditions. Pt/MgAl<sub>2</sub>O<sub>4</sub> also showed higher thermal stability up to 800 °C and lower stability of sulfur-containing species.

© 2010 Elsevier Inc. All rights reserved.

## 1. Introduction

NO<sub>x</sub> storage-reduction (NSR) has gained considerable importance as an efficient method for exhaust gas treatment of fuel lean engines, which operate at air-to-fuel ratios higher than stoichiometric (>14.7–25). Under such conditions, exhaust NO<sub>x</sub> is oxidized over a noble metal and then trapped (stored) on alkaline-earth or alkali metal components in the form of metal nitrates. During the subsequent short fuel-rich period, stored NO<sub>x</sub> are reduced to N<sub>2</sub>, and the storage-reduction cycle restarts [1,2]. Conventional NSR catalysts are thus made up of three main components: (i) a noble metal for NO<sub>x</sub> oxidation and reduction, (ii) a NO<sub>x</sub> storage component and (iii) a suitable oxidic support for dispersion of the noble metal and storage component. The original standard NSR catalyst formulation is Pt–Ba/Al<sub>2</sub>O<sub>3</sub> [3,4]. However, under realistic conditions, particularly at short regeneration times, storage performance deteriorates with time (from cycle to cycle) due to incomplete reduction of bulk barium nitrates that are partially inaccessible during subsequent lean phase, an issue surprisingly little investigated [5–11]. Also, deterioration of the storage performance is observed with Ba-containing catalyst due to mixed oxide formation [12,13]. At high temperatures, Ba can react with Al<sub>2</sub>O<sub>3</sub> to form BaAl<sub>2</sub>O<sub>4</sub> or with Pt to form BaPtO<sub>3</sub>, which are believed to be the key species for lowering the storage activity [14,15]. CO<sub>2</sub>, which is an

unavoidable exhaust component in practice, is believed to play a detrimental role in the storage performance of Pt–Ba/Al<sub>2</sub>O<sub>3</sub> catalyst [16–19]. Sulfur poisoning is another problem encountered with Ba-containing catalysts: SO<sub>2</sub> in the exhaust gas can be oxidized on precious metals and react with the storage component, forming barium sulfate. Because sulfates are more stable than nitrates, they hamper the NO<sub>x</sub> storage (adsorption), thus deactivating the catalyst [20,21].

Therefore, improvement of the conventional catalyst formulation is highly desirable, particularly in regard to dynamic storage-reduction performance, thermal stability and sulfur tolerance. Takahashi et al. synthesized Pt–K/MgAl<sub>2</sub>O<sub>4</sub>, in which the spinel (MgAl<sub>2</sub>O<sub>4</sub>) support could enhance the basicity of the potassium used as storage component, resulting in a higher amount of stored NO<sub>x</sub> at higher temperature [22]. Attempts toward Ba- or K-free NSR catalyst formulations also have been made. Hydrotalcites (Mg<sub>x</sub>Al<sub>y</sub>O<sub>z</sub> where x/y > 2) without any classical storage material showed promising storage activity at lower temperatures, and NO<sub>x</sub> sorption over these catalysts was primarily a surface phenomenon without the generation of bulk species [23–26]. The hydrotalcites, however, experienced sintering of Pt<sup>0</sup> and formation of MgAl<sub>2</sub>O<sub>4</sub> from Mg(A–l)O mixed oxide during thermal or hydrothermal aging. Both effects resulted in a loss of NO<sub>x</sub> storage capacity.

Here, we report the single-step flame synthesis of 1 wt.% Pt/MgAl<sub>2</sub>O<sub>4</sub>, a new type of NSR catalyst that does not contain conventional storage materials and shows superior dynamic NSR performance at short regeneration times and higher thermal stability compared to a standard reference catalyst, 1 wt.% Pt–20% Ba/Al<sub>2</sub>O<sub>3</sub>.

\* Corresponding author. Fax: +41 44 632 1163.  
E-mail address: [baiker@chem.ethz.ch](mailto:baiker@chem.ethz.ch) (A. Baiker).

## 2. Experimental

### 2.1. Catalyst preparation

One weight percentage of Pt/MgAl<sub>2</sub>O<sub>4</sub> was synthesized by flame spray pyrolysis (FSP) [27]. The precursor solution was aluminum (III) acetylacetonate (ABCR Chemicals, 99%), magnesium (II) tert-butoxide (Alfa Aesar, 94%) and platinum (II) acetylacetonate (ABCR Chemicals, 99.9%) dissolved in a 1:1 vol.% mixture of methanol and acetic acid. The precursor solution was fed at 5 cc min<sup>-1</sup> through the nozzle with the help of a syringe pump. The formed solid particles were collected on a glass fiber filter with the aid of a vacuum pump. For comparison, a standard reference catalyst, 1wt.% Pt–20% Ba/Al<sub>2</sub>O<sub>3</sub>, was prepared by incipient wetness impregnation method [28]. The reference catalyst 1 wt.% Pt–Ba/Al<sub>2</sub>O<sub>3</sub> was prepared by impregnation of a 1 wt.% Pt/Al<sub>2</sub>O<sub>3</sub> catalyst with an aqueous solution of Ba acetate. One weight percentage of Pt–Mg/Al<sub>2</sub>O<sub>3</sub> was also prepared by similar way (using Mg acetate as precursor). The dried material was pretreated *in situ* at 500 °C and cooled to 350 °C at which temperature NSR cycles were performed.

### 2.2. Catalyst characterization

The structural properties of the synthesized powders were characterized by X-ray diffraction, TEM and STEM, <sup>27</sup>Al MAS NMR, and nitrogen adsorption measurements using the BET method. X-ray diffraction was carried out on a Siemens D5000 diffractometer, using CuK<sub>α1</sub> ( $\lambda = 1.54056 \text{ \AA}$ ) in step mode from 15° to 65° (2 $\theta$ ) with 0.01° step size and 0.3 s step<sup>-1</sup>.

For TEM and STEM, the material was dispersed in ethanol and deposited onto a perforated carbon foil supported on a copper grid. The investigations were performed on a Tecnai F30 microscope (FEI (Eindhoven); field emission cathode, operated at 300 kV). TEM images were recorded with a slow-scan charge-coupled device camera.

Nitrogen physisorption isotherms (adsorption–desorption branches) were measured on a Micromeritics ASAP 2000 instrument at 77 K. Samples were outgassed under vacuum at 150 °C before measurement, and the specific surface area (SSA) was determined using the BET method.

<sup>27</sup>Al MAS NMR experiments (Bruker Avance 700) were performed at room temperature in a 2.5-mm double-resonance probe-head spinning at 15 kHz. The spectra were deconvoluted using 1D WINNMR software.

CO chemisorption was performed with a Micromeritics ASAP 2010C instrument. The sample was exposed to a hydrogen flow at 350 °C for 1 h and then evacuated at the same temperature. Two chemisorption isotherms were then measured at room temperature. The first isotherm corresponds to all carbon monoxide adsorbed on the catalyst. After evacuation at the same temperature for 1 h, the second isotherm was measured, corresponding to the weakly adsorbed CO. From the difference between the two isotherms, the fraction of strongly adsorbed (chemisorbed) CO on Pt surfaces, denoted as CO<sub>a</sub>/Pt, was determined. The stoichiometric factor (number of CO molecules per Pt site) was assumed to be 1. In the literature, 0.7 [29] and 1 [27] have been proposed for similar systems.

NO<sub>x</sub> and SO<sub>x</sub> storage properties of the catalysts were evaluated by pulse thermal analysis (TA) using Netzsch, Jupiter 449. The samples were heated to 500 °C in a constant flow of 50 cc min<sup>-1</sup> of 6 vol.% O<sub>2</sub>/He and subsequently cooled to 250 °C. After obtaining a stable TG baseline at this temperature, NO pulses (2 cc) were admitted to the system in 15-min intervals. SO<sub>x</sub> storage was measured in the same way. Temperature-programmed desorption (TPD) was performed after saturating the materials. Saturation

experiments were carried out specifically at 250 °C, because at higher temperature, there was desorption of NO<sub>x</sub> from the catalyst. TPD was performed in a thermobalance up to 1200 °C with a heating rate of 10 °C min<sup>-1</sup> under flowing He (50 cc min<sup>-1</sup>).

Time-resolved *in-situ* DRIFT spectra were measured at 250 °C by flowing 1000 ppm of NO + 6.6 vol.% O<sub>2</sub>/He over the powder catalysts placed in a plug-flow cell [30,31]. The vibrational spectra were collected with a Bruker Equinox 55 spectrometer equipped with a liquid-nitrogen-cooled MCT detector at 4 cm<sup>-1</sup> resolution.

### 2.3. Catalytic tests

The NSR experiments were carried out isothermally at 250 and 350 °C with 100 mg of the 100–200  $\mu\text{m}$  sieve fraction of the catalysts in a vertically placed plug-flow quartz reactor. Temperature was calibrated by positioning a thermocouple in the center of the reactor. The gases were introduced via mass flow controllers, and the effluent gases were analyzed using mass spectrometer (Thermostar™, Pfeiffer Vacuum). The reactor was connected to a valve, which allowed rapid switching between oxidizing (lean) and reducing (rich) atmospheres. The rich period consisted of 5 vol.% H<sub>2</sub>/He or CO/He or C<sub>3</sub>H<sub>6</sub>/He (varied from 10 s to 120 s), whereas the lean period consisted of 1000 ppm of NO in 6.6 vol.% O<sub>2</sub>/He (for 360 s). To explore the effect of CO<sub>2</sub>, additionally 5 vol.% CO<sub>2</sub> were feed in the lean period. The specific reaction conditions have been mentioned in respective places. The total flow rate was 120 cc min<sup>-1</sup>.

## 3. Results and discussion

### 3.1. Structural properties of catalysts

The XRD patterns of the as-prepared 1 wt.% Pt/MgAl<sub>2</sub>O<sub>4</sub> showed the reflections of the spinel MgAl<sub>2</sub>O<sub>4</sub> (Fig. 1A). A minor reflection at 40° 2 $\theta$  was observed due to some larger Pt crystallites. The average crystallite size of the spinel estimated by the Scherrer equation was 12 nm. The XRD pattern of Pt–Ba/Al<sub>2</sub>O<sub>3</sub> showed prominent BaCO<sub>3</sub> reflections along with a reflection around 40° 2 $\theta$  due to  $\gamma$ -Al<sub>2</sub>O<sub>3</sub> (Fig. 1B). Note that this reflection coincides with a possible reflection of Pt at the same position. However, XRD analysis of pure alumina clearly showed that the observed reflection is mainly due to the alumina. Detailed structural investigation of Pt–Ba/Al<sub>2</sub>O<sub>3</sub> has been reported previously from our group [14,15,32]. STEM investigations (Fig. 1G) revealed that Pt and MgAl<sub>2</sub>O<sub>4</sub> were predominantly present as less than 3-nm and 12-nm particles, respectively (a typical TEM image is shown in Supplementary material Fig. S1). However, also some larger Pt (~10 nm) and MgAl<sub>2</sub>O<sub>4</sub> (>50 nm) particles were found indicating a bimodal particle size distribution of Pt and MgAl<sub>2</sub>O<sub>4</sub>. These larger Pt particles gave rise to the weak XRD reflection at 40° 2 $\theta$ . The bimodal particle size distribution is likely the result of the solvent mixture used in the flame synthesis and can be related to the combustion enthalpy of the methanol/acetic acid mixture in flame spray pyrolysis [33,34]. Fig. 1H represents a typical STEM image of the spent 1 wt.% Pt/MgAl<sub>2</sub>O<sub>4</sub> (after 50 NSR cycles at 350 °C). No noticeable difference was observed between the fresh and the spent catalyst. The BET surface area of as-prepared 1 wt.% Pt/MgAl<sub>2</sub>O<sub>4</sub> was 226 m<sup>2</sup> g<sup>-1</sup>, which is comparable to the highest specific surface areas reported for MgAl<sub>2</sub>O<sub>4</sub> in literature [35]. On the other hand, the BET surface area of the reference Pt–Ba/Al<sub>2</sub>O<sub>3</sub> catalyst was 128 m<sup>2</sup> g<sup>-1</sup>. Solid-state <sup>27</sup>Al MAS NMR of Pt/MgAl<sub>2</sub>O<sub>4</sub> revealed that a significant amount of the aluminum was in a tetrahedral position. Considering the formula for inverse spinels, (Mg<sub>1-x</sub>Al<sub>x</sub>)(Mg<sub>x</sub>Al<sub>2-x</sub>)O<sub>4</sub>, values for  $x$  of 0.63 and 0.64 were found for the as-prepared and the spent catalyst, respectively. CO chemisorption performed on Pt–Ba/Al<sub>2</sub>O<sub>3</sub>

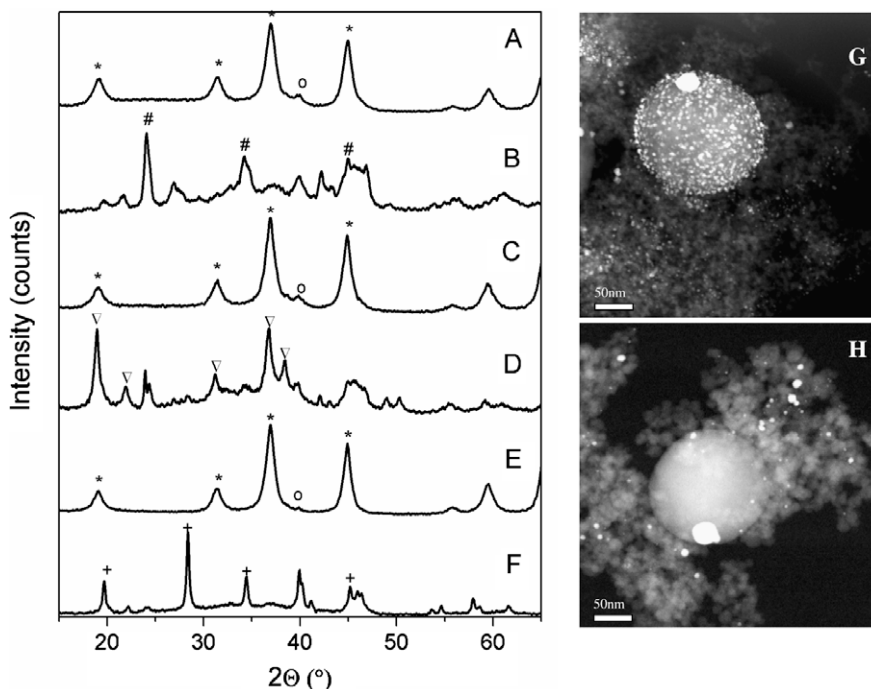


**Fig. 1.** XRD profile of (A) as-prepared 1% Pt/MgAl<sub>2</sub>O<sub>4</sub>; (B) as-prepared 1% Pt–Ba/Al<sub>2</sub>O<sub>3</sub>; (C) NO<sub>x</sub>-treated 1% Pt/MgAl<sub>2</sub>O<sub>4</sub>; (D) NO<sub>x</sub>-treated 1% Pt–Ba/Al<sub>2</sub>O<sub>3</sub>; (E) 1% Pt/MgAl<sub>2</sub>O<sub>4</sub> after pretreatment at 1000 °C; and (F) 1% Pt–Ba/Al<sub>2</sub>O<sub>3</sub> after pretreatment at 1000 °C (\*, MgAl<sub>2</sub>O<sub>4</sub>; ○, Pt; #, BaCO<sub>3</sub>; ∇, Ba(NO<sub>3</sub>)<sub>2</sub>; and +, BaAl<sub>2</sub>O<sub>4</sub>). (G) and (H) represent typical STEM images of as-prepared and spent (after 50 NSR cycles at 350 °C) 1 wt.% Pt/MgAl<sub>2</sub>O<sub>4</sub>, respectively.

and Pt/MgAl<sub>2</sub>O<sub>4</sub> showed a CO/Pt ratio of 0.44 for the former [30] and 0.13 for the latter. Assuming similar stoichiometry for CO adsorption on Pt for the two catalysts, we infer that the Pt-dispersion in Pt–Ba/Al<sub>2</sub>O<sub>3</sub> was significantly higher than in Pt/MgAl<sub>2</sub>O<sub>4</sub>, probably due to the higher heat impact during the flame synthesis.

### 3.2. NSR performance

Fig. 2A compares the NO<sub>x</sub> concentration (ppm) at the reactor outlet during the dynamic storage–reduction cycling over 1 wt.% Pt/MgAl<sub>2</sub>O<sub>4</sub> and the reference 1 wt.% Pt–Ba/Al<sub>2</sub>O<sub>3</sub>, respectively, at 350 °C. No pretreatment was carried out with the catalysts. Initially, the reference catalyst outperformed the spinel-based catalyst, storing almost all NO during the first two cycles, while the 1 wt.% Pt/MgAl<sub>2</sub>O<sub>4</sub> stored about 90 % of NO during the first cycle. After the first cycle, the storage behavior deteriorated for both catalysts. However, a more prominent drop of storage performance with the cycles was observed for the reference catalyst compared to the Pt/MgAl<sub>2</sub>O<sub>4</sub>. The NO<sub>x</sub> storage amount under these dynamic reaction conditions after 10 cycles (constant up to 50 cycles) was 78% for Pt/MgAl<sub>2</sub>O<sub>4</sub>, whereas the reference catalyst showed only 58% NO<sub>x</sub> storage (Fig. 2B). A similar result was obtained by carrying out the experiment at 250 °C (not shown). During reduction, there was huge formation of N<sub>2</sub>, accompanied by a very small evolution of NH<sub>3</sub> at the end of the rich span over both the catalysts (Supplementary material, Fig. S2). However, over Pt/MgAl<sub>2</sub>O<sub>4</sub>, initially there was a small amount of N<sub>2</sub>O formation, which was not observed for the reference catalyst. It should be mentioned in this context that we have also performed similar NSR cycling experiments over a 1 wt.% Pt–Mg/Al<sub>2</sub>O<sub>3</sub> catalyst prepared by depositing MgO on Pt/Al<sub>2</sub>O<sub>3</sub> (where no spinel phase was formed), which showed only 40% of NO<sub>x</sub> storage after 10 cycles (Supplementary material, Fig. S3). This comparative test clearly indicated that the presence of the spinel phase is crucial for high catalytic performance. The higher NO<sub>x</sub> storage efficiency of the spinel catalyst with H<sub>2</sub> as reductant at short reduction time is evidenced in Fig. 3. NSR

cycles were performed at 350 °C over the two catalysts using five different rich time periods (10–120 s) (the lean period was kept constant at 360 s). It can be observed that given a higher reduction time, Ba-based catalyst outperformed the Pt/MgAl<sub>2</sub>O<sub>4</sub>. However, when the rich periods were small (10, 20 and 30 s), the storage over Pt/MgAl<sub>2</sub>O<sub>4</sub> was better compared to the reference catalyst.

### 3.3. Storage capacity

The total NO<sub>x</sub> storage amount was determined gravimetrically by saturating both Pt/MgAl<sub>2</sub>O<sub>4</sub> and Pt–Ba/Al<sub>2</sub>O<sub>3</sub> by NO<sub>x</sub> at 250 °C. Desorption was carried out up to 1000 °C, and the NO MS traces were calibrated by NO injections at 1000 °C. Interestingly, the thus determined saturation uptake of the Ba-based catalyst was almost four times higher than the one of Pt/MgAl<sub>2</sub>O<sub>4</sub> (inset of Fig. 4). Furthermore, the TPD profile of Pt–Ba/Al<sub>2</sub>O<sub>3</sub> (Fig. 4) reflects more complex features than that of Pt/MgAl<sub>2</sub>O<sub>4</sub>, which could be associated with the formation of different nitrate/nitrite species and will be discussed in the following section. In the TPD experiments, Pt/MgAl<sub>2</sub>O<sub>4</sub> showed a maximal rate of desorption at 437 °C, whereas Pt–Ba/Al<sub>2</sub>O<sub>3</sub> exhibited two broad maxima around ca. 413 and 486 °C. Thus, it can be concluded that Pt–Ba/Al<sub>2</sub>O<sub>3</sub> has higher storage capacity, and the phase containing stored NO<sub>x</sub> is thermally more stable than that in Pt/MgAl<sub>2</sub>O<sub>4</sub>. However, during dynamic cycling with more realistic short reduction periods, this apparent advantage is not reflected in better NSR performance.

### 3.4. Nature of stored species

Fig. 5 shows the time-resolved DRIFT spectra of Pt–Ba/Al<sub>2</sub>O<sub>3</sub> and Pt/MgAl<sub>2</sub>O<sub>4</sub>, respectively. As reported previously, several bands assigned to nitrites and nitrates emerged for the Ba-based catalyst. The initial band at 1240 cm<sup>−1</sup> (which is assignable to the ν<sub>3</sub> vibration of Ba-nitrite [36]) shifted to 1300 cm<sup>−1</sup> with time. The major band at 1300 cm<sup>−1</sup> is due to the formation of ionic Ba-nitrate with time [36–39]. The sharp band at 1770 cm<sup>−1</sup> is attributed to bulk

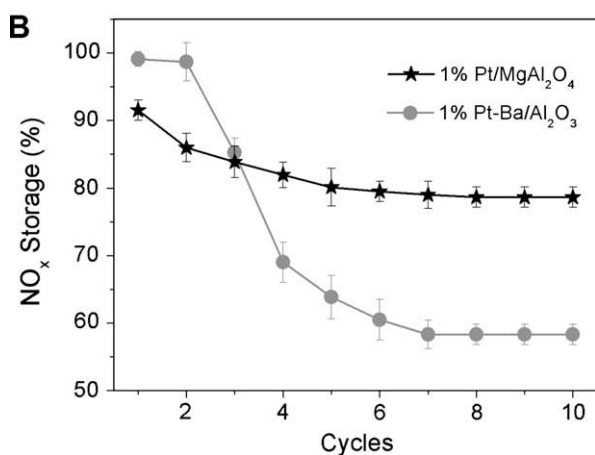
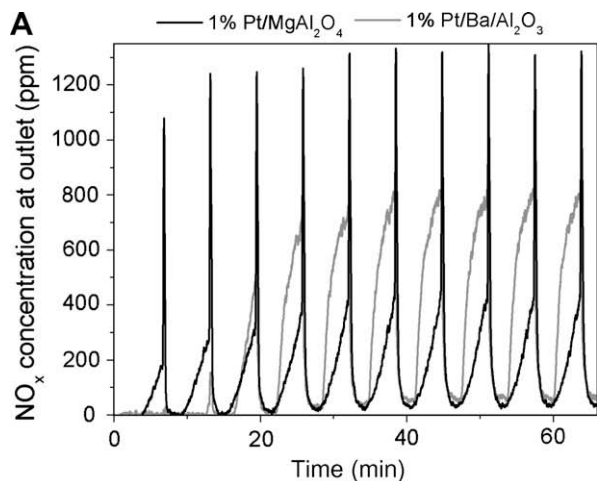


**Fig. 2.** (A) Concentration of  $\text{NO}_x$  (ppm) at the reactor outlet during NSR cycling over  $\text{Pt}/\text{MgAl}_2\text{O}_4$  and the reference 1%  $\text{Pt}-\text{Ba}/\text{Al}_2\text{O}_3$  standard catalyst, respectively. Lean period was 360 s, and rich period was 20 s. The storage amount reached a stable value after the 7th cycle, which was maintained during the test of up to 50 cycles. Here, for clarity, the data are plotted only up to 10 cycles. (B) The percentage of  $\text{NO}_x$  storage over the two catalysts with the consecutive cycles.

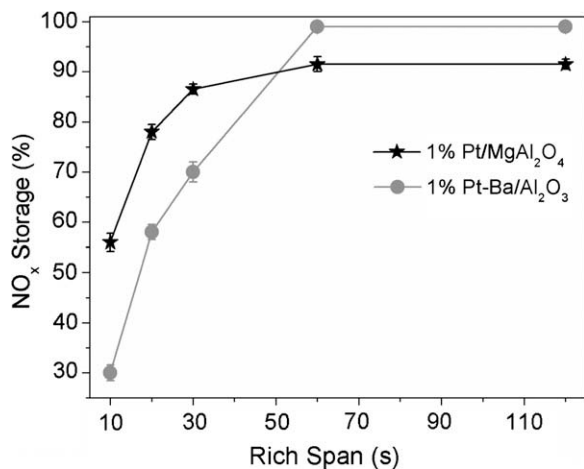


**Fig. 3.** The amount of  $\text{NO}_x$  storage during NSR cycles at 350 °C over 1 wt.%  $\text{Pt}/\text{MgAl}_2\text{O}_4$  and the reference 1 wt.%  $\text{Pt}-\text{Ba}/\text{Al}_2\text{O}_3$  catalyst pretreated with different rich period using  $\text{H}_2$  as reductant. The NSR cycles were carried out with 360 s lean and 10, 20, 30, 60 and 120 s rich spans. The storage amounts plotted are the values obtained after 10 steady cycles.

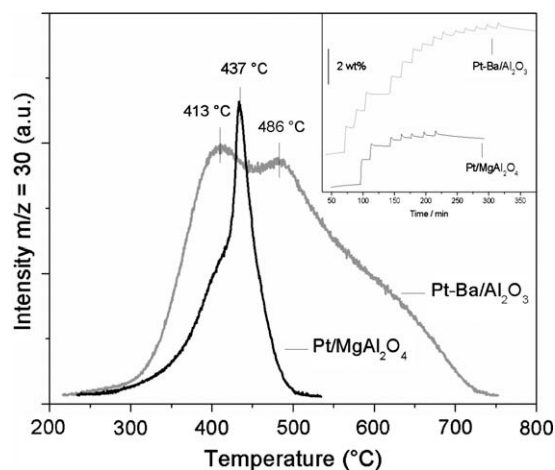


**Fig. 4.** Temperature-programmed desorption (TPD) of catalysts previously saturated with  $\text{NO}_x$  by pulsing  $\text{NO}$  in 6 vol.%  $\text{O}_2/\text{He}$  atmosphere at 250 °C. Integration of the  $m/z = 30$  areas showed that the 1 wt.%  $\text{Pt}-\text{Ba}/\text{Al}_2\text{O}_3$  had a four times larger total uptake under these conditions than the 1 wt.%  $\text{Pt}/\text{MgAl}_2\text{O}_4$ . The corresponding sorption curves are shown in inset.

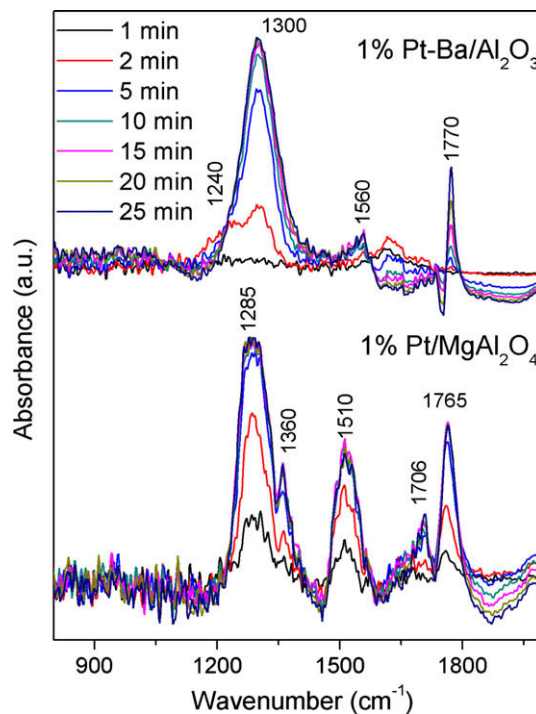


**Fig. 5.** Time-resolved DRIFT spectra of  $\text{NO}_x$  adsorption by flowing 1000 ppm of  $\text{NO} + 6.6$  vol.%  $\text{O}_2/\text{He}$  over 1 wt.%  $\text{Pt}-\text{Ba}/\text{Al}_2\text{O}_3$  and 1 wt.%  $\text{Pt}/\text{MgAl}_2\text{O}_4$  at 250 °C.

$\text{Ba}-\text{nitrate}$  [38]. The band at 1560  $\text{cm}^{-1}$  is assigned to nitrate species formed on  $\text{Al}_2\text{O}_3$ , and the two negative bands at 1650 and 1750  $\text{cm}^{-1}$  are probably attributable to the decomposition of  $\text{Ba}-\text{carbonate}$  during  $\text{NO}_x$  adsorption [38,39]. The time-resolved vibrational spectra of  $\text{Pt}/\text{MgAl}_2\text{O}_4$  were significantly different from that of  $\text{Pt}-\text{Ba}/\text{Al}_2\text{O}_3$ . The lower panel of Fig. 5 shows two major bands at 1285 and 1510  $\text{cm}^{-1}$ . These two bands are assigned to the surface-bound chelating bidentate nitrate [39–42]. Unlike  $\text{Pt}-\text{Ba}/\text{Al}_2\text{O}_3$ , no nitrite band was observed for spinel-based catalyst, indicating a very fast  $\text{NO}$  oxidation. Some surface monodentate nitrates (1360  $\text{cm}^{-1}$ ) and bridging bidentate nitrates (1706  $\text{cm}^{-1}$ ) were also formed [39,41]. The other major band at 1765  $\text{cm}^{-1}$  could be attributed to adsorbed  $\text{N}_2\text{O}_4$  (or  $\text{NO}^+\text{NO}_3^-$ ) [40,43]. We can

conclude from the time-resolved DRIFT study that (i) NO oxidation over Pt/MgAl<sub>2</sub>O<sub>4</sub> is faster than on Pt-Ba/Al<sub>2</sub>O<sub>3</sub> and (ii) Pt-Ba/Al<sub>2</sub>O<sub>3</sub> forms bulk Ba-nitrate, whereas the spinel-based catalyst predominantly forms surface nitrates. The formation of bulk Ba(NO<sub>3</sub>)<sub>2</sub> over Pt-Ba/Al<sub>2</sub>O<sub>3</sub> was also confirmed by XRD analysis after exposure of the catalysts to NO and O<sub>2</sub> at 250 °C for 2 h (Fig. 1D). The XRD profile of the NO<sub>x</sub>-treated Pt/MgAl<sub>2</sub>O<sub>4</sub> in Fig. 1C does not show any reflection of bulk Mg(NO<sub>3</sub>)<sub>2</sub>. Thus, *in-situ* time-resolved DRIFT and XRD investigation indicated that bulk nitrate species were formed on Pt-Ba/Al<sub>2</sub>O<sub>3</sub>, whereas on the spinel-based catalyst, only evidence of surface species was found. The same conclusion also emerged from ATR-IR measurements (see Supplementary material Fig. S4). This different kind of adsorption over the two catalysts is also reflected in the difference in the TPD profiles of the two catalysts. The different thermal stability of the surface Ba-nitrite, ionic Ba-nitrate and Al-nitrate lead to a complex TPD profile of Pt-Ba/Al<sub>2</sub>O<sub>3</sub> with broad and multiple maxima.

Apparently, there is a significantly different mode of adsorption of NO<sub>x</sub> on Pt/MgAl<sub>2</sub>O<sub>4</sub> when compared to Pt-Ba/Al<sub>2</sub>O<sub>3</sub>, with the latter producing a substantial amount of bulk-like species after NO-adsorption. The presence of bulk nitrate species in NSR usually results in poorer performance of the catalyst due to limited diffusion of reductants into the bulk and semi-bulk species [44–46]. Therefore, the lack of bulk nitrate species after adsorption on Pt/MgAl<sub>2</sub>O<sub>4</sub> could explain the better dynamic storage-reduction performance. During storage-reduction cycles, within a shorter regeneration span of 10 or 20 s, complete reduction of surface nitrates occurred over Pt/MgAl<sub>2</sub>O<sub>4</sub>, whereas over the Ba-based catalyst, only the surface nitrates were reduced, keeping the semi-bulk and bulk Ba(NO<sub>3</sub>)<sub>2</sub> unaltered due to the diffusion limitation mentioned above. Consequently, after a certain number of cycles, the bulk Ba species in the Pt-Ba/Al<sub>2</sub>O<sub>3</sub> catalyst remained inaccessible for storage resulting in a poorer storage performance, whereas Pt/MgAl<sub>2</sub>O<sub>4</sub> showed superior dynamic storage-reduction performance in short rich periods that are normally used in technical applications.

### 3.5. Influence of type of reductant

To mimic the realistic gas mixture, many researchers have used other reductants such as CO or hydrocarbons (HC) for Pt-Ba/Al<sub>2</sub>O<sub>3</sub> catalysts. Among these three reducing agents, H<sub>2</sub> is by far the best reductant, and the efficiency of reductant follows H<sub>2</sub> > CO > HC [47–49]. The effect of different reductants was

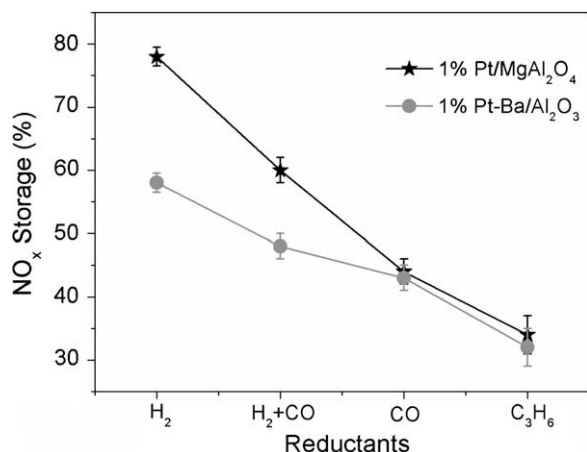


**Fig. 6.** Amount of NO<sub>x</sub> storage during NSR using different reductants. The NSR cycles at 350 °C were carried out with 360 s lean and 20 s rich spans. The rich period consisted of 5 vol.% H<sub>2</sub>/He, or 5 vol.% CO/He or 5 vol.% H<sub>2</sub>/He + CO/He or 5 vol.% C<sub>3</sub>H<sub>6</sub> and the lean period of 1000 ppm of NO in 6.6 vol.% O<sub>2</sub>/He.

explored on the new spinel catalyst in terms of stored NO<sub>x</sub>. Fig. 6 shows the amount of NO<sub>x</sub> storage by using H<sub>2</sub>, CO + H<sub>2</sub>, CO and C<sub>3</sub>H<sub>6</sub> as reductant. The reduction efficiency was H<sub>2</sub> > H<sub>2</sub>+CO > CO > C<sub>3</sub>H<sub>6</sub> over both catalysts in accordance with literature. It is interesting to note that using H<sub>2</sub> as a reductant, Pt/MgAl<sub>2</sub>O<sub>4</sub> showed better efficiency, whereas CO and C<sub>3</sub>H<sub>6</sub> resulted in similar NSR performance for both catalysts. CO is believed to be adsorbed on Pt sites according to the following reaction: CO + Pt → CO-Pt and CO-Pt + Pt → C-Pt + O-Pt and eventually poisons the Pt sites by depositing C onto it. C<sub>3</sub>H<sub>6</sub> can also poison the Pt sites in a similar way. NO in the lean phase can remove the deposited C on Pt sites by two ways: either by direct reaction, C-Pt + NO → CO + N-Pt followed by N-Pt + 2O → NO<sub>2</sub>, or by oxidation of NO to NO<sub>2</sub> on Pt sites and reaction of the formed NO<sub>2</sub> with C, leading to the formation of CO<sub>2</sub> and NO [50–52]. On the contrary, inhibition effect of CO on Pt sites is a well-known fact [53]. CO poisons the precious metal sites by strong adsorption and thereby inhibits not only NO oxidation and reduction, but also nitrate decomposition. The exact elucidation of these processes was out of the scope of this study, but it seems that CO and C<sub>3</sub>H<sub>6</sub> poison both catalysts in a similar fashion.

### 3.6. Effect of CO<sub>2</sub>

CO<sub>2</sub>, originating from fuel combustion, can influence the NO storage behavior of NSR catalysts. Studies on Pt-Ba/Al<sub>2</sub>O<sub>3</sub> revealed

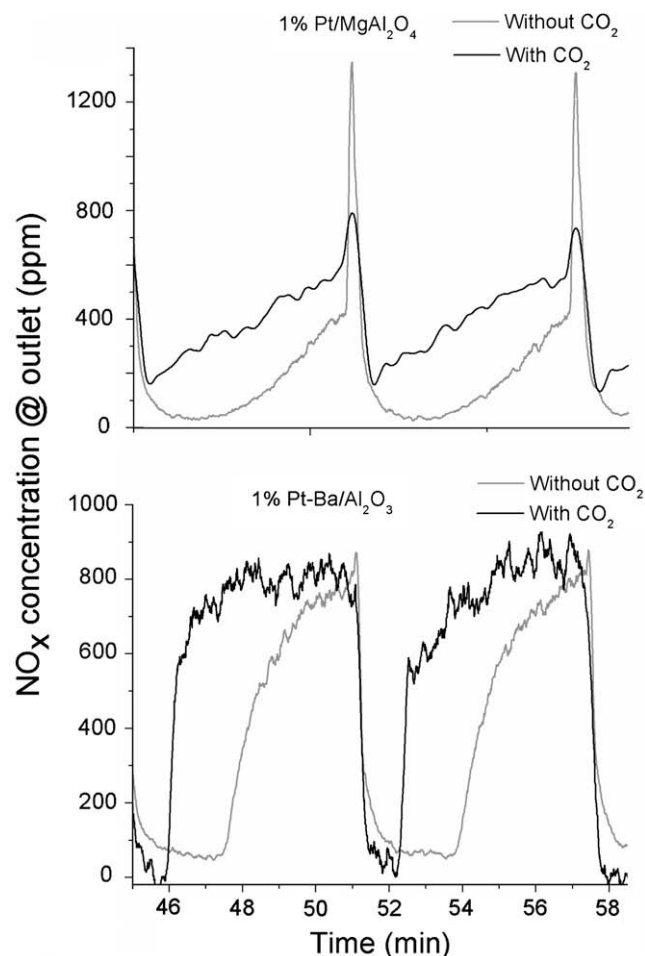


**Fig. 7.** Concentration of NO<sub>x</sub> (ppm) at the reactor outlet during NSR cycling (with 360 s lean and 20 s rich span) at 350 °C over Pt/MgAl<sub>2</sub>O<sub>4</sub> (upper panel) and the reference standard catalyst Pt-Ba/Al<sub>2</sub>O<sub>3</sub> (lower panel) in presence of CO<sub>2</sub> (black line) and in absence of CO<sub>2</sub> (gray line).

that  $\text{CO}_2$  competes with  $\text{NO}_x$  for the basic sites of metal oxides and forms a large variety of carbonate species thus resulting in a detrimental effect on the storage efficiency of the catalyst [16–19]. Therefore, its influence on the storage behavior of  $\text{Pt}/\text{MgAl}_2\text{O}_4$  and  $\text{Pt}-\text{Ba}/\text{Al}_2\text{O}_3$  was investigated. Fig. 7 shows the different  $\text{NO}_x$  profile during NSR in the presence and in the absence of 5 vol.%  $\text{CO}_2$  over  $\text{Pt}-\text{Ba}/\text{Al}_2\text{O}_3$  and  $\text{Pt}/\text{MgAl}_2\text{O}_4$ . The storage efficiency of  $\text{Pt}-\text{Ba}/\text{Al}_2\text{O}_3$  diminished from 58% to 33%, while that of  $\text{Pt}/\text{MgAl}_2\text{O}_4$  decreased from 78% to 56% in presence of  $\text{CO}_2$ . The performances of both catalysts were affected negatively by the presence of  $\text{CO}_2$  in the gas-stream, but  $\text{Pt}/\text{MgAl}_2\text{O}_4$  was relatively less affected, which could be a significant advantage in technical applications.

### 3.7. Thermal stability

Another important issue regarding technical applications is the thermal stability of the NSR material. To explore the thermal stability of the  $\text{Pt}/\text{MgAl}_2\text{O}_4$ , the  $\text{NO}_x$  storage performance was evaluated after catalyst pretreatment at elevated temperatures.  $\text{Pt}/\text{MgAl}_2\text{O}_4$  as well as the reference catalyst was pretreated at four different temperatures (700, 800, 900, and 1000 °C) for 8 h, and the NSR test cycles were performed with these catalysts (Supplementary material, Fig. S5). Fig. 8 shows the amount of  $\text{NO}_x$  stored on both catalysts previously exposed to different temperatures. The  $\text{NO}_x$  storage amount over  $\text{Pt}/\text{MgAl}_2\text{O}_4$  was almost similar up to 800 °C and then deteriorated gradually. The storage performance of the reference catalyst deteriorated drastically with increasing pretreatment temperature. The XRD patterns of pretreated  $\text{Pt}/\text{MgAl}_2\text{O}_4$  were almost unchanged, except that the spinel reflections became sharper indicating larger spinel crystallites and the appearance of distinct Pt reflections (Fig. 1E). The diminished storage efficiency of high temperature pretreated  $\text{Pt}/\text{MgAl}_2\text{O}_4$  can be attributed to the loss of surface area due to heat pretreatment (see the SSA in Fig. 8). The reference catalyst also lost its initial surface area, but to a lower extent. However, it is known to form a substantial amount of  $\text{BaAl}_2\text{O}_4$  (Fig. 1F) under these conditions, which lowers the  $\text{NO}_x$  storage capacity [14,15].

### 3.8. Effect of sulfur poisoning

Next, we investigated the tolerance of both catalysts toward sulfur poisoning. This was carried out by alternative injection of

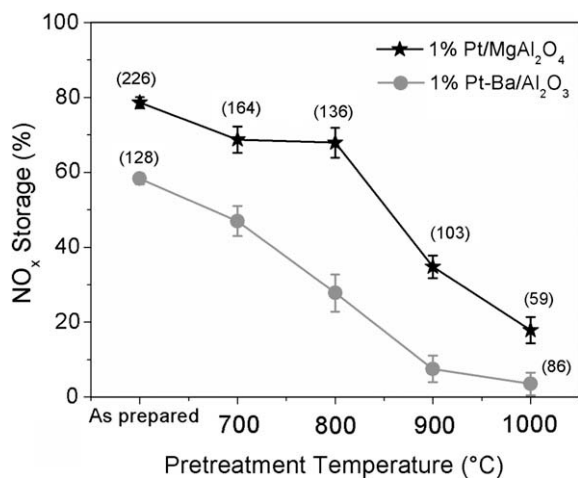


**Fig. 8.** Amount of  $\text{NO}_x$  stored during NSR cycles over 1 wt.%  $\text{Pt}/\text{MgAl}_2\text{O}_4$  and the reference 1 wt.%  $\text{Pt}-\text{Ba}/\text{Al}_2\text{O}_3$  catalyst pretreated at different temperatures. NSR cycles were carried out with 360 s lean and 20 s rich span. The rich period consisted of 5 vol.%  $\text{H}_2/\text{He}$ , and the lean period of 1000 ppm of  $\text{NO}$  in 6.6 vol.%  $\text{O}_2/\text{He}$ . The storage values were calculated after reaching a steady state. The BET surface area (in  $\text{m}^2 \text{g}^{-1}$ ) of 1 wt.%  $\text{Pt}/\text{MgAl}_2\text{O}_4$  measured after NSR cycles is given in parentheses.

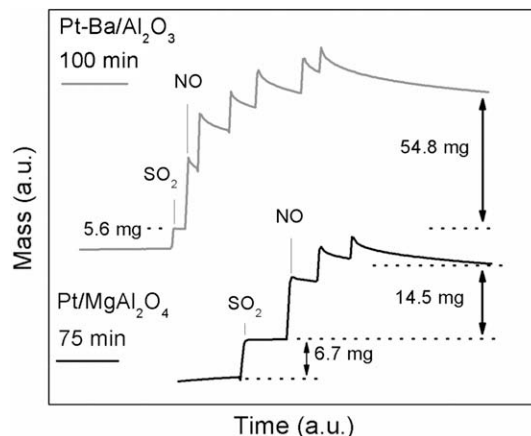


**Fig. 9.** Poisoning with  $\text{SO}_2$  and subsequent  $\text{NO}_x$  adsorption on 1 wt.%  $\text{Pt}-\text{Ba}/\text{Al}_2\text{O}_3$  and 1 wt.%  $\text{Pt}/\text{MgAl}_2\text{O}_4$ , respectively. Note the different time scales of both experiments. The amount of  $\text{NO}_x$  adsorbed was not determined gravimetrically, but by calibration of the amount of  $\text{NO}$  desorbed during heating to 900 °C. The amounts of  $\text{NO}_x$  and  $\text{SO}_x$  stored on the catalysts are indicated in mg per gram of the catalyst.

2 cc  $\text{O}_2$  and 2 cc 10%  $\text{SO}_2/\text{He}$  at 250 °C. Subsequent to the poisoning, the catalysts were exposed to alternative  $\text{NO}$  (2 cc) and  $\text{O}_2$  (2 cc) injections. Fig. 9 shows the adsorption of  $\text{SO}_2$  and subsequent adsorption of  $\text{NO}_x$  on both catalysts.  $\text{Pt}/\text{MgAl}_2\text{O}_4$  took up a somewhat higher amount of  $\text{SO}_2$  ( $6.7 \text{ mg g}^{-1}$ ) when compared to the reference catalyst ( $5.6 \text{ mg g}^{-1}$ ), which is not surprising in view of the much larger surface area of this catalyst ( $226$  compared to  $128 \text{ m}^2 \text{ g}^{-1}$ ). The amount of  $\text{NO}_x$  adsorbed after saturating the materials amounted to  $14.5 \text{ mg g}^{-1}$  for  $\text{Pt}/\text{MgAl}_2\text{O}_4$  and  $54.8 \text{ mg g}^{-1}$  for  $\text{Pt}-\text{Ba}/\text{Al}_2\text{O}_3$ . The latter was determined by calibration of the integrated  $\text{NO}$  signal during desorption up to 900 °C. Thermogravimetric analysis showed a  $\text{NO}_x$  uptake of  $25 \text{ mg g}^{-1}$  for the fresh  $\text{Pt}/\text{MgAl}_2\text{O}_4$  catalyst, whereas  $\text{Pt}-\text{Ba}/\text{Al}_2\text{O}_3$  showed  $96 \text{ mg NO}_x$  uptake per gram of the catalyst (see Fig. 4 inset). Interestingly, the relative loss of stored  $\text{NO}_x$  after  $\text{SO}_x$  poisoning was similar for both catalysts (41% for  $\text{Pt}/\text{MgAl}_2\text{O}_4$  and 43% for the reference catalyst).

TPD of  $\text{SO}_x$ -saturated  $\text{Pt}/\text{MgAl}_2\text{O}_4$  and  $\text{Pt}-\text{Ba}/\text{Al}_2\text{O}_3$  revealed striking differences in  $\text{SO}_2$  desorption behavior. Fig. 10 shows the desorption behavior of  $\text{SO}_2$  from both samples (after saturating

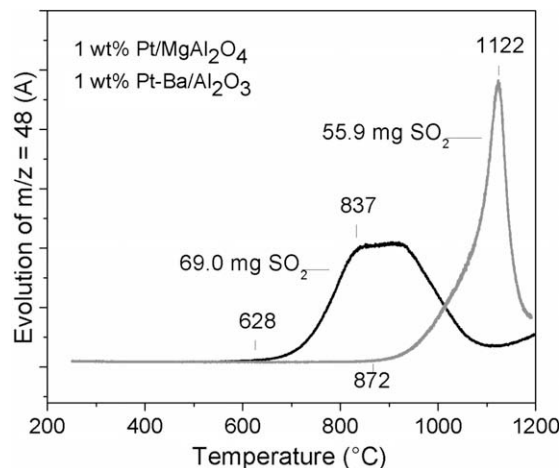


**Fig. 10.** Temperature-programmed desorption from 1 wt.%  $\text{Pt}-\text{Ba}/\text{Al}_2\text{O}_3$  and 1 wt.%  $\text{Pt}/\text{MgAl}_2\text{O}_4$  previously saturated with  $\text{SO}_x$  by pulsing alternatively 2 cc  $\text{O}_2$  and 2 cc 10%  $\text{SO}_2/\text{He}$  mixture.

the catalysts by alternative SO<sub>2</sub> and O<sub>2</sub> pulses) by monitoring the *m/z* = 48 evolution by MS. The total uptake was 69.0 mg SO<sub>x</sub> for Pt/MgAl<sub>2</sub>O<sub>4</sub> and 55.9 mg for Pt–Ba/Al<sub>2</sub>O<sub>3</sub>. Pt/MgAl<sub>2</sub>O<sub>4</sub> started desorbing SO<sub>2</sub> at 628 °C reaching a broad maximum at around 837 °C. Pt–Ba/Al<sub>2</sub>O<sub>3</sub> on the other hand showed desorption starting at 872 °C and reached a maximum at 1122 °C. This clearly indicates that the sulfates formed on the Ba-based catalyst are thermally much more stable and thus more difficult to decompose compared to those formed on the spinel. Note that under the conditions applied in the sulfur poisoning experiment, Pt/MgAl<sub>2</sub>O<sub>4</sub> adsorbed more SO<sub>x</sub> than the conventional catalyst. XRD analysis of Pt/MgAl<sub>2</sub>O<sub>4</sub> saturated by SO<sub>x</sub> showed no crystalline Mg sulfates (not shown). Apparently, reaction of SO<sub>x</sub> with Pt/MgAl<sub>2</sub>O<sub>4</sub> resulted in an amorphous sulfur-containing phase, which could explain the broad desorption peak of SO<sub>2</sub> of this material.

#### 4. Conclusions

Our comparative study of flame-derived Pt/MgAl<sub>2</sub>O<sub>4</sub> and a Pt–Ba/Al<sub>2</sub>O<sub>3</sub> reference revealed a superior dynamic NO<sub>x</sub> storage-reduction behavior at short regeneration times for Pt/MgAl<sub>2</sub>O<sub>4</sub>. The spinel-based Pt/MgAl<sub>2</sub>O<sub>4</sub> catalyst is free of any additional conventional storage materials (Ba, K). It can be produced by a single-step flame spray pyrolysis, which is easily scalable and reproducible. Also, direct decomposition of flame-made materials on ceramic foams has been demonstrated [54], rendering technical application feasible. XRD and IR studies indicate the absence of bulk NO<sub>x</sub> species after storage, suggesting that NO<sub>x</sub> are mainly stored on the spinel surface. This seems to be a characteristic property of Pt/MgAl<sub>2</sub>O<sub>4</sub> and enables improved NSR efficiency at short regeneration (reduction) times. However, this improved efficiency was only observed with H<sub>2</sub>, while with other reductants such as CO or HC, similar behavior at short regeneration times was observed for both Pt/MgAl<sub>2</sub>O<sub>4</sub> and the reference Pt–Ba/Al<sub>2</sub>O<sub>3</sub> catalyst. Addition of CO<sub>2</sub> to the feed-stream and high-temperature treatment resulted in a decrease in the NSR capacity of the spinel-based Pt/MgAl<sub>2</sub>O<sub>4</sub>, but this decrease was far less than that observed for the reference Pt–Ba/Al<sub>2</sub>O<sub>3</sub>, suggesting that the Pt/MgAl<sub>2</sub>O<sub>4</sub> is competitive under demanding conditions. Preliminary sulfur poisoning experiments showed a similar relative loss of NO<sub>x</sub> uptake for Pt/MgAl<sub>2</sub>O<sub>4</sub> and the reference catalyst. However, on Pt/MgAl<sub>2</sub>O<sub>4</sub>, the formed sulfates showed strikingly lower thermal stability compared to that on the reference catalyst. The spinel-based catalyst also exhibited higher thermal stability up to 800 °C compared to the reference Pt–Ba/Al<sub>2</sub>O<sub>3</sub> catalyst.

#### Acknowledgments

We kindly acknowledge financial support by ETH Zurich (TH-09 06-2). Thanks are due to Frank Krumeich for the electron microscopy investigations. Electron microscopy was performed at EMEZ (Electron Microscopy ETH Zurich).

#### Appendix A. Supplementary material

Supplementary data associated with this article can be found, in the online version, at [doi:10.1016/j.jcat.2010.02.017](https://doi.org/10.1016/j.jcat.2010.02.017).

#### References

- [1] W.S. Epling, L.E. Campbell, A. Yezerets, N.W. Currier, J.E. Parks, Catal. Rev. Sci. Eng. 46 (2004) 163.

- [2] S. Roy, A. Baiker, Chem. Rev. 109 (2009) 4054.  
 [3] S. Matsumoto, Catal. Today 29 (1996) 43.  
 [4] N. Takahashi, H. Shinjoh, T. Iijima, T. Suzuki, K. Yamazaki, K. Yokota, H. Suzuki, N. Miyoshi, S. Matsumoto, T. Tanizawa, T. Tanaka, S. Tateishi, K. Kasahara, Catal. Today 27 (1996) 63.  
 [5] R. Burch, Catal. Rev. 46 (2004) 271.  
 [6] Y. Li, S. Roth, J. Dettling, T. Beutel, Top. Catal. 16/17 (2001) 139.  
 [7] W.S. Epling, A. Yezerets, N.W. Currier, Catal. Lett. 110 (2006) 143.  
 [8] J.-S. Choi, W.P. Partridge, C.S. Daw, Appl. Catal. A 293 (2005) 24.  
 [9] J.-S. Choi, W.P. Partridge, C.S. Daw, Appl. Catal. B 77 (2007) 145.  
 [10] N. Takahashi, K. Yamazaki, H. Sobukawa, H. Shinjoh, Appl. Catal. B 70 (2007) 198.  
 [11] J.P. Breen, C. Rioche, R. Burch, C. Hardacre, F.C. Meunier, Appl. Catal. B 72 (2007) 178.  
 [12] T. Szailer, J.H. Kwak, D.H. Kim, J. Szanyi, C.M. Wang, C.H.F. Peden, Catal. Today 114 (2006) 86.  
 [13] D.H. Kim, Y.H. Chin, J.H. Kwak, C.H.F. Peden, Catal. Lett. 124 (2008) 39.  
 [14] M. Casapu, J.-D. Grunwaldt, M. Maciejewski, M. Wittrock, U. Göbel, A. Baiker, Appl. Catal. B 63 (2006) 232.  
 [15] M. Casapu, J.-D. Grunwaldt, M. Maciejewski, A. Baiker, R. Hoyer, M. Wittrock, S. Eckhoff, Catal. Lett. 120 (2008) 1.  
 [16] W.S. Epling, G.C. Campbell, J.E. Parks, Catal. Lett. 90 (2003) 45.  
 [17] W.S. Epling, J.E. Parks, G.C. Campbell, A. Yezerets, N.W. Currier, L.E. Campbell, Catal. Today 96 (2004) 21.  
 [18] C.M.L. Scholz, V.R. Gangwal, M.H.J.M. de Croon, J.C. Schouten, Appl. Catal. B 71 (2007) 143.  
 [19] L. Lietti, P. Forzatti, I. Nova, E. Tronconi, J. Catal. 204 (2001) 175.  
 [20] H. Abdulhamid, E. Fridell, J. Dawody, J. Dawody, M. Skoglundh, J. Catal. 241 (2006) 200.  
 [21] A. Amberntsson, M. Skoglundh, S. Ljungstrom, E. Fridell, J. Catal. 217 (2003) 253.  
 [22] N. Takahashi, S. Matsunaga, T. Tanaka, H. Sobukawa, H. Shinjoh, Appl. Catal. B 77 (2007) 73.  
 [23] G. Fornasari, F. Trifiro, A. Vaccari, F. Prinetto, G. Ghiotti, G. Centi, Catal. Today 75 (2002) 421.  
 [24] G. Centi, G.E. Arena, S. Perathoner, J. Catal. 216 (2003) 443.  
 [25] G. Fornasari, R. Glockler, M. Livi, A. Vaccari, Appl. Clay Sci. 29 (2005) 258.  
 [26] B.A. Silletti, R.T. Adams, S.M. Sigmon, A. Nikolopoulos, J.J. Spivey, H.H. Lamb, Catal. Today 114 (2006) 64.  
 [27] R. Strobel, L. Madler, M. Piacentini, M. Maciejewski, A. Baiker, S.E. Pratsinis, Chem. Mater. 18 (2006) 2532.  
 [28] M. Piacentini, M. Maciejewski, A. Baiker, Appl. Catal. B 60 (2005) 265.  
 [29] J. Dawody, L. Eurenus, H. Abdulhamid, M. Skoglundh, E. Olsson, E. Fridell, Appl. Catal. A 296 (2005) 157.  
 [30] N. Maeda, A. Urakawa, A. Baiker, J. Phys. Chem. C 113 (2009) 16724.  
 [31] A. Urakawa, N. Maeda, A. Baiker, Angew. Chem. Int. Ed. 47 (2008) 9256.  
 [32] M. Casapu, J.-D. Grunwaldt, M. Maciejewski, A. Baiker, S. Eckhoff, U. Göbel, M. Wittrock, J. Catal. 251 (2007) 28.  
 [33] L. Mädler, W.J. Stark, S.E. Pratsinis, J. Mater. Res. 17 (2002) 1356.  
 [34] N. van Vegten, D. Ferri, M. Maciejewski, F. Krumeich, A. Baiker, J. Catal. 249 (2007) 269.  
 [35] W.C. Li, M. Comotti, A.H. Lu, F. Schüth, Chem. Commun. (2006) 1772.  
 [36] I. Nova, L. Castoldi, F. Prinetto, V. Dal Santo, L. Lietti, E. Tronconi, P. Forzatti, G. Ghiotti, R. Psaro, S. Recchi, Top. Catal. 30/31 (2004) 181.  
 [37] I. Malpartida, M.O. Guerrero-Pérez, M.C. Herrera, M.A. Larrubia, L.J. Alemany, Catal. Today 126 (2007) 162.  
 [38] H. Hesse, A. Urakawa, A. Baiker, J. Phys. Chem. C 113 (2009) 12286.  
 [39] C. Sedlmair, K. Seshan, A. Jentys, J.A. Lercher, J. Catal. 214 (2003) 308.  
 [40] J.J. Yu, Z. Jiang, L. Zhu, Z.P. hao, Z.P. Xu, J. Phys. Chem. B 110 (2006) 4291.  
 [41] S. Morandi, F. Prinetto, G. Ghiotti, M. Livi, A. Vaccari, Micropor. Mesopor. Mater. 107 (2008) 31.  
 [42] F. Prinetto, G. Ghiotti, I. Nova, L. Lietti, E. Tronconi, P. Forzatti, J. Phys. Chem. B 105 (2001) 12732.  
 [43] I. Perdana, D. Creaser, O. Ohrman, J. Hedlund, J. Catal. 234 (2005) 219.  
 [44] C.M.L. Scholz, V.R. Gangwal, M.H.J.M. de Croon, J.C. Schouten, J. Catal. 245 (2007) 215.  
 [45] R.L. Muncrief, P. Khanna, K.S. Kabin, M.P. Harold, Catal. Today 98 (2004) 393.  
 [46] X. Chen, J. Schwank, J. Li, W.F. Schneider, C.T. Goralski Jr., P.J. Schmitz, Appl. Catal. B 61 (2005) 164.  
 [47] T. Szailer, J.H. Kwak, D.H. Kim, J.C. Hanson, C.H.F. Peden, J. Szanyi, J. Catal. 239 (2006) 51.  
 [48] P. Jozsa, E. Jobson, M. Larsson, Top. Catal. 30/31 (2004) 177.  
 [49] D. James, E. Fourre, M. Ishii, M. Bowker, Appl. Catal. B: Environ. 45 (2003) 147.  
 [50] C.M.L. Scholz, B.H.W. Maes, M.H.J.M. de Croon, J.C. Schouten, Appl. Catal. A 332 (2007) 1.  
 [51] L. Castoldi, R. Matarrese, L. Lietti, P. Forzatti, Appl. Catal. B 64 (2006) 25.  
 [52] J.A. Sullivan, O. Keane, A. Cassidy, Appl. Catal. B 75 (2007) 102.  
 [53] M. AL-Harbi, W.S. Epling, Appl. Catal. B 89 (2009) 315.  
 [54] B. Schimmoeller, H. Schulz, S.E. Pratsinis, A. Bareiss, A. Reitzmann, B.K. Czarnetzki, J. Catal. 243 (2006) 82.